Inorganic Chemistry

Article

pubs.acs.org/IC

N-Heterocyclic Phosphenium Ligands as Sterically and Electronically-Tunable Isolobal Analogues of Nitrosyls

Baofei Pan, Zhequan Xu, Mark W. Bezpalko, Bruce M. Foxman, and Christine M. Thomas*

Department of Chemistry, Brandeis University, 415 South Street MS 015, Waltham, Massachusetts 02454, United States

Supporting Information

ABSTRACT: The coordination chemistry of an N-heterocyclic phosphenium (NHP)-containing bis(phosphine) pincer ligand has been explored with Pt^0 and Pd^0 precursors. Unlike previous compounds featuring monodentate NHP ligands, the resulting NHP Pt and Pd complexes feature pyramidal geometries about the central phosphorus atom, indicative of a stereochemically active lone pair. Structural, spectroscopic, and computational data suggest that the unusual pyramidal NHP geometry results from two-electron reduction of the phosphenium ligand to generate transition metal complexes in which the Pt or Pd centers have been formally oxidized by two electrons. Interconversion between planar and pyramidal NHP geometries can be affected by either coordination/dissociation of a two-electron donor ligand or two-electron redox processes, strongly supporting an isolobal analogy with the linear (NO^+) and bent (NO^-) variations of nitrosyl ligands. In contrast to nitrosyls, however, these new main group noninnocent ligands are sterically and electronically tunable and are amenable to incorporation into chelating ligands, perhaps representing a new strategy for promoting redox transformations at transition metal complexes.

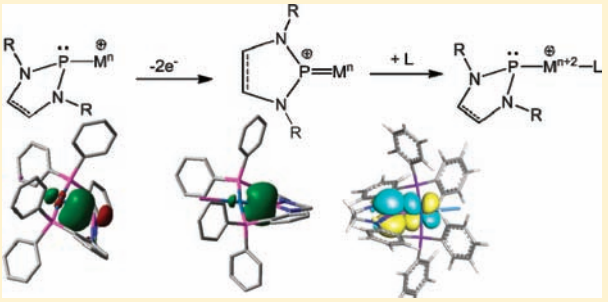

INTRODUCTION

Since the isolation of the first stable N-heterocyclic carbene (NHC) by Arduengo and co-workers in 1991,[1] NHCs have been widely studied in the field of transition metal chemistry[2−4] and catalysis.[5,6] As the "carbon copies" of NHCs, far less attention has been paid to their isovalent group 15 analogues, N-heterocyclic phosphenium cations (NHP^+s).[7−9] In contrast to NHCs, which are considered to be strong σ-donors and weak-π acceptors, theoretical investigations of the electronic properties of NHP cations have shown that their bonding is dominated by π-acceptor character, with only weak σ-donation to the transition metal.[10−12] Owing to the electronically inverse properties of these two ligand families, NHPs are expected to exhibit reciprocal reactivity in transition metal chemistry.

One of the most interesting aspects of NHP^+ cations is their analogy to NO^+ in coordination chemistry, not only because of both ligands' cationic charge but also because of their similar ability to adopt two different transition metal binding modes (Chart 1). Most commonly, when binding to electron poor metal fragments, NHPs adopt a planar geometry at the phosphorus atom, acting as both σ donors and π acceptors and resulting in a metal−phosphorus double bond (e.g., $Cp(CO)_2Mo(NHP^{Me})$).[13] On the other hand, when binding to electron rich metal fragments, NHPs adopt a pyramidal geometry, which suggests that there is a nonbonding lone pair on the central phosphorus atom (e.g., $Cp^*(CO)_2Fe(NHP^{Me})$).[14] This leads to two limiting descriptions: (1) the electrophilic phosphenium is acting exclusively as a two-electron acceptor ligand to the metal (NHP^+/M^n), or (2) the NHP has formally oxidized the metal center and is acting as an X-type phosphido-ligand (NHP^-/M^{n+2}). In this sense, a convincing analogy between NHPs and nitrosyls can be

Chart 1. Analogy between NHPs and Nitrosyls in Coordination Chemistry

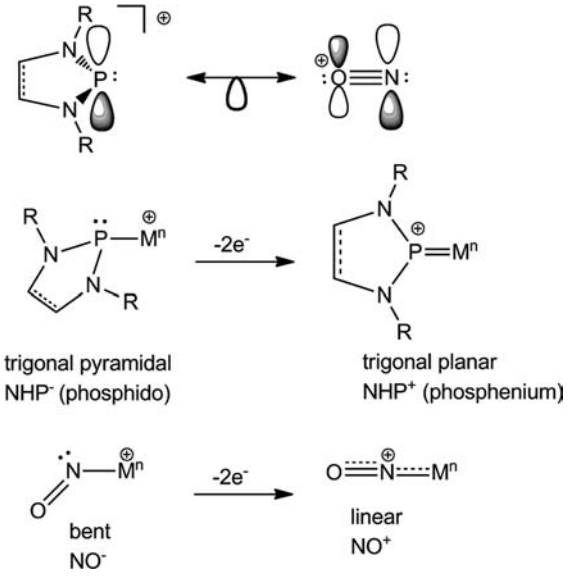

Received: November 30, 2011
Published: March 14, 2012

   dx.doi.org/10.1021/ic202581v | Inorg. Chem. 2012, 51, 4170−4179

established, highlighting the potential noninnocent behavior of these ligands. Key advantages of NHPs over their nitrosyl counterparts are the ability to tune steric and electronic properties via derivatization and the ability to incorporate these ligands into chelating frameworks. These strategies may also impart stability to metal NHP complexes and protect the phosphenium unit from nucleophilic attack.

The ability of NHPs to adopt a different binding mode with vastly different donor/acceptor properties may enhance the redox activity of transition metal NHP complexes. Given the analogy to nitrosyl ligands, which can undergo a two electron redox transformation ($NO^+ + 2e^- \rightarrow NO^-$),[15] such redox interconversion is also anticipated to be applicable for NHPs. There are examples of transition metal complexes containing both planar and pyramidal NHP ligands in the literature;[13,14] however, to the best of our knowledge, there is no report of interconversion between these two species via two electron redox chemistry. Gudat and co-workers proposed a pyramidal-to-planar conformational change via the loss of a CO ligand ($(NHP)Co(CO)_4 \rightarrow (NHP)Co(CO)_3$), but the pyramidal geometry of the NHP in $(NHP)Co(CO)_4$ was not structurally confirmed.[16] Incorporation of NHPs into chelating ligands should prove advantageous in stabilizing transition metal species with different NHP binding modes; however, in contrast to a rapidly growing number of NHC-containing chelating ligands in transition metal chemistry,[17,18] multidentate ligands featuring NHPs are noticeably absent from the literature.

Recently our group reported the synthesis and characterization of the first example of an NHP-containing pincer ligand in which the central NHP unit is linked to two phosphine side arms via aryl linkers.[19] The coordination of this pincer-NHP ligand to transition metal halide starting materials proved problematic as a result of the tendency of halides to migrate to the electrophilic NHP center to form halophosphine complexes.[19] A successful route to NHP-metal complexes was realized via sodium halide extrusion from the anionic metal complex $Na[Co(CO)_4]$ and a chlorophosphine precursor to generate $[PPP]Co(CO)_2$ (PPP = NHP-diphosphine ligand).[20] Attempts to promote a pyramidal-to-planar interconversion of the NHP via CO extrusion from $[PPP]Co(CO)_2$ was unsuccessful.[20] Herein, we turn our attention to treatment of the $[PPP]^+$ ligand with halide-free Pd^0 and Pt^0 starting materials, uncovering more support for the analogy with nitrosyl ligands, namely, ligand conformational changes promoted by redox changes or coordination of additional two-electron donor ligands.

RESULTS AND DISCUSSION

Phosphenium Ligand Addition to M^0 Starting Materials. Treatment of the ligand $[PPP]^+$ with $Pd(PPh_3)_4$ at room temperature for 12 h generates the Pd dimer $[(PPP)Pd]_2[PF_6]_2$ (**1**, Scheme 1). The ^{31}P NMR spectrum of **1** features a downfield signal at 288.3 ppm and an upfield signal at 14.1 ppm in a 1:2 integral ratio, which is consistent with a coordinated central NHP unit and two coordinated aryl phosphine arms. The solid state structure of **1** reveals an asymmetric geometry. As shown in Figure 1, each Pd center has a short bond to one of the NHP phosphorus atoms (Pd–P102: 2.1616(15) Å) and an elongated contact to the other NHP phosphorus atom (Pd–P102′: 2.4982(16) Å). The short $P^{(NHP)}$–Pd bond is consistent with double bond character and comparable to the $P^{(NHP)}$–Pd distances in the two

Scheme 1

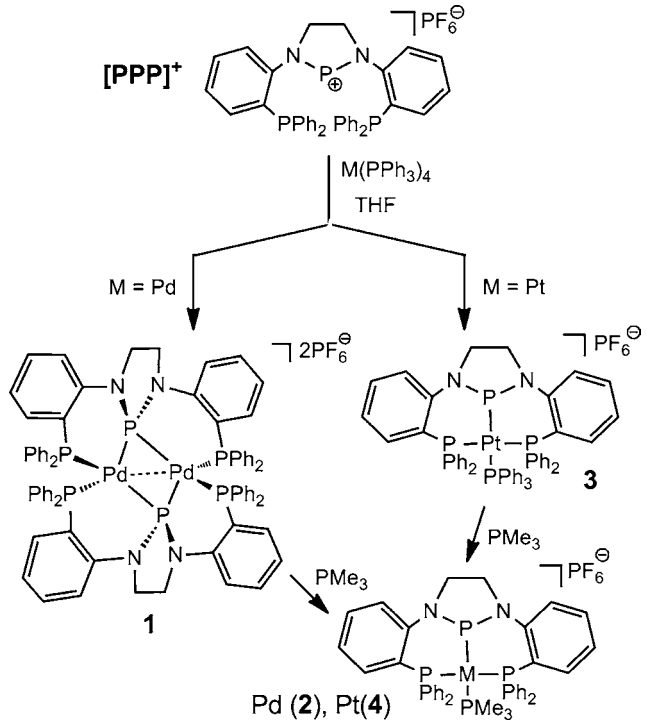

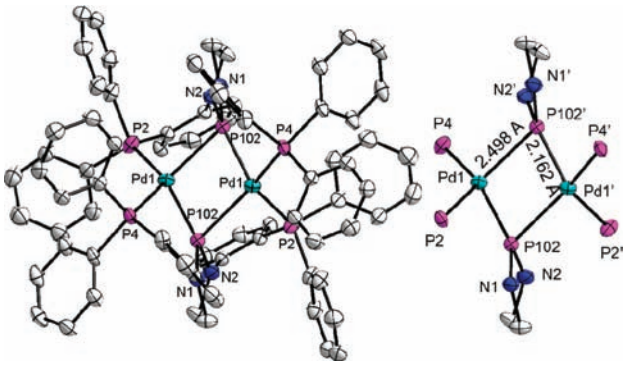

Figure 1. Displacement ellipsoid (50%) representation of **1**. For clarity the PF_6^- counterions and all hydrogen atoms have been omitted. Relevant interatomic distances (Å) and angles (deg): **1**: Pd1–Pd1′, 2.7500(5); Pd1–P102, 2.1616(15); Pd1–P102′, 2.4982(16); Pd1–P2, 2.3547(8); Pd1–P4′, 2.3659(8); P2–Pd1–P4′, 122.24(3); P2–Pd1–P102, 84.54(4); P102–Pd1–P102′, 104.85(5); P102′–Pd1-P4, 84.66(4); P2–Pd1–P102′, 123.31(5); P4–Pd1–P102, 140.84(4).

structurally characterized Pd-NHP complexes reported by Jones and co-workers (2.1227(10) Å, 2.1167(25) Å).[21] In complex **1**, each NHP moiety acts as an NHP^+ phosphenium ligand toward one Pd center, with a nearly planar angle (164.5°) between the N–P–N plane and the short $P^{(NHP)}$–Pd bond vector. The other Pd center weakly donates electron density into the empty p orbital on the same central phosphorus, resulting in an elongated bonding interaction along with a bent angle (122.5°) between the N–P–N plane and the long $P^{(NHP)}$–Pd bond vector (Figure 2). These geometric features can be best attributed to a semibridging NHP arrangement, analogous to a semibridging carbonyl ligand. The tetrahedral geometry of both Pd centers is in agreement with the NHP^+ phosphenium Pd^0 assignment for **1**.

dx.doi.org/10.1021/ic202581v | Inorg. Chem. 2012, 51, 4170–4179

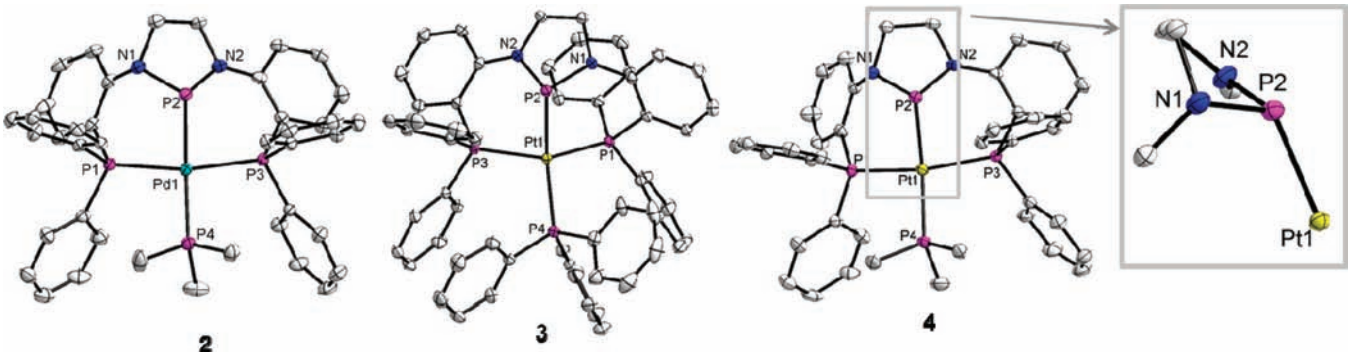

Figure 2. Displacement ellipsoid (50%) representation of **2**, **3**, and **4**. For clarity, all hydrogen atoms, PF_6^- counteranions, and solvate molecules have been omitted. Relevant interatomic distances (Å) and angles (deg): **2**: Pd–P2, 2.2535(6); Pd–P1, 2.3099(5); Pd–P3, 2.3384(5); Pd–P4, 2.4148(5); P1–Pd–P2, 86.128(23); P2–Pd–P3, 83.307(23); P3–Pd–P4, 97.750(22); P1–Pd–P4, 98.041(22); P1–Pd–P3, 161.993(19); P2–Pd–P4, 154.619(20). **3:** P2–Pt, 2.2600(7); P1–Pt, 2.3137(7); P3–Pt, 2.3190(6); P4–Pt, 2.3787(6); P1–Pt–P2, 86.081(23); P2–Pt–P3, 81.367(23); P3–Pt–P4, 102.287(21); P1–Pt–P4, 103.973(21); P1–Pt–P3, 147.173(22); P2–Pt–P4, 149.086(22). **4:** P2–Pt, 2.2606(9); P1–Pt, 2.3025(10); P3–Pt, 2.3123(11); P4–Pt, 2.367(1); P1–Pt–P2, 87.418(51); P2–Pt–P3, 84.453(50); P3–Pt–P4, 96.573(44); P1–Pt–P4, 96.912(44); P1–Pt–P3, 163.388(37); P2–Pt–P4, 154.962(33).

The Pd dimer **1** can be broken into the monomer complex $[(PPP)Pd(PMe_3)][PF_6]$ (**2**) by treatment with PMe_3 (Scheme 1). In comparison to **1**, the ^{31}P NMR shift of the central phosphorus atom in **2** is shifted more upfield (235.6 ppm). Structural characterization of monomer **2** reveals that the central phosphorus adopts a pyramidal geometry with a bent angle of 130.9° between the N–P–N plane and the $P^{(NHP)}$–Pd bond vector. In addition, the $P^{(NHP)}$–Pd bond distance is considerably longer (2.2535(6) Å) than the short $P^{(NHP)}$–Pd double bond distance in **1** (2.16316(15) Å), indicative of a Pd–P single bond in **2**. On the basis of literature precedent, the pyramidal NHP unit in **2** can be described as either an NHP^+ phosphenium ligand accepting electron density from a Pd^0 center or an NHP^- phosphido ligand covalently bound to a Pd^{II} center.[14,16,20] Given the nearly square planar geometry of the Pd center in **2**, the latter phosphide description appears to be more reasonable. Moreover, the Pd–$P^{(NHP)}$ distance in **2** is essentially identical to the central Pd–P distance in a recently reported phosphido-diphosphine pincer ligand complex of Pd (2.2533(9) Å).[22] While the Pd^{II} center is not rigorously square planar, this is likely the result of steric factors, and computational results are consistent with the phosphide description (vide infra). Thus, NHP^+ phosphenium (**1**) and NHP^- phosphido (**2**) transition metal binding modes can be interconverted simply by dissociation or association of an additional two-electron donor.

In contrast to the Pd case, treatment of the $[PPP]^+$ ligand with $Pt(PPh_3)_4$ does not lead to the formation of a Pt dimer similar to **1**. Instead, the reaction cleanly generates the four-coordinate monomer complex $[(PPP)Pt(PPh_3)][PF_6]$ (**3**, Scheme 1). Here, the ^{31}P NMR spectrum features a downfield signal at 198.8 ppm and two upfield shifts at 29.1 and 13.6 ppm, which are consistent with a coordinated NHP unit coupled to two Pt-bound aryl phosphine arms and one ligated triphenylphosphine ligand, respectively. Interestingly, the central $P^{(NHP)}$-Pt coupling constant ($^1J_{Pt-P}$ = 445 Hz) is substantially smaller compared to all five reported NHP-Pt^0 complexes in the literature (ranging from 6162 to 7354 Hz),[23,24] but within the range of bis(phosphine)phosphido-Pt^{II} complexes reported by Mazzeo and co-workers (648 to 2790 Hz).[25] This suggests that the central NHP in **3** is adopting a pyramidal geometry and acting as an NHP^- phosphido ligand.

The solid state structure of **3** is shown in Figure 2, and, as expected from the ^{31}P NMR spectrum, the geometry at the central phosphorus is unequivocally pyramidal, with a bent angle of 126.2° between the N–P–N plane and the $P^{(NHP)}$-Pt bond vector. The $P^{(NHP)}$-Pt bond distance in **3** (2.2600(7) Å) is significantly longer compared to reported NHP-Pt^0 complexes (2.1073(9) Å,[23] 2.116(3) Å[24]), and in line with the phosphide Pt^{II}–P distances in the diphosphino-phosphide pincer ligand complexes reported by Mazzeo et al. (2.3091(14) Å, 2.2573(11) Å).[25] Similar to **2**, the Pt metal center in **3** adopts a distorted square planar geometry. Thus, the NHP unit in **3** is best described as an NHP^- phosphido ligand, and the Pt center is best described as divalent Pt^{II}. The distorted geometry about Pt is attributed, like the aforementioned Pd case, to steric factors. Indeed, there are no examples of square planar PPh_3-coordinated complexes with aryl linked bis(diarylphosphine) pincer ligands in the literature for comparison. The coordinated PPh_3 in **3** can be replaced by PMe_3 to generate $[(PPP)Pt(PMe_3)][PF_6]$ (**4**), which is isostructural to **2**. Because of the smaller cone angle of PMe_3 in comparison to PPh_3, the Pt geometry in **4** is less distorted from ideal square planar than in **3** (Figure 2).

Addition of P-X bonds to M^0 Starting Materials. The oxidative addition of C-X (X = halide) bonds to Pd^0 precursors has proven to be a useful method for the synthesis of NHC-Pd^{II} complexes.[26,27] Pd^{II} phosphide fragments can also be generated via oxidative addition of P–Cl bonds to Pd^0.[28] Jones and co-workers reported the addition of a bromophosphine NHP precursor to a Pd^0 center to generate the first example of a structurally characterized Pd^0 halide via heterolytic (non-oxidative) addition of the $P^{(NHP)}$-Br bond to Pd^0.[21] Similarly, our ligand precursors [PPP]-X also react with M^0 (Pd/Pt) starting materials to afford neutral four-coordinate complexes, (PPP)Pd-X (X = Cl (**5**), Br (**6**), I (**7**)) and (PPP)Pt-X (X = Cl (**8**), Br (**9**), I (**10**)), via the addition of the $P^{(NHP)}$–X bond across the metal center, as shown in Scheme 2. The ease of $P^{(NHP)}$–X bond cleavage is consistent with Gudat's description of increasing ionic Lewis acid–base pair character of the $P^{(NHP)}$–X bond in the order $I^- > Br^- > Cl^-$.[9] The ^{31}P NMR spectrum for each of the [PPP]-M-X complexes features one downfield central phosphorus resonance (246–250 ppm for **5**–**7**, 219–225 ppm for **8**–**10**) and one upfield peak for the phosphine side arms (6.1–7.5 ppm for **5**–**7**, 9.4–12.1 ppm for

dx.doi.org/10.1021/ic202581v | Inorg. Chem. 2012, 51, 4170–4179

Scheme 2

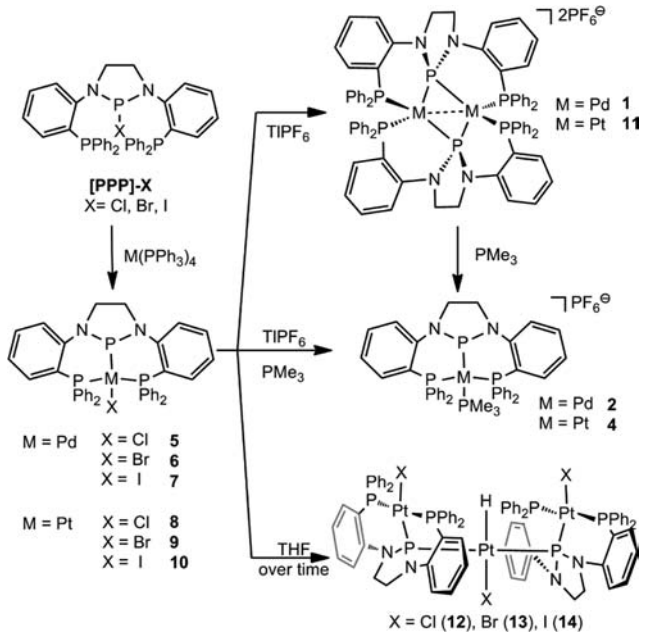

8–**10**) in an integral ratio of 1:2. All three $P^{(NHP)}$-Pt coupling constants observed for complexes **8**–**10** are notably small (486, 607, 663 Hz) in contrast to reported NHP^+ phosphenium Pt complexes,[23,24] but consistent with those in complex **3** (445 Hz) and **4** (496 Hz), suggesting a pyramidal NHP geometry with NHP^- phosphide character in complexes **5**–**10**.

As predicted, the solid state structures of **5** and **9** reveal pyramidal geometries with respect to the central phosphorus atom (angles between the N–P–N plane and $P^{(NHP)}$–Pd bond vector: 119.1° (**5**); 120.8° (**9**)) and the metal centers are rigorously square planar rather than the tetrahedral geometry that would be expected for d^{10}-M^0 complexes (Figure 3). Thus, the $P^{(NHP)}$–X addition reactions shown in Scheme 2 are best described as formal oxidative addition processes, and the NHPs here are best described as NHP^- phosphido ligands bound to Pt^{II}. This assignment is consistent with the relatively long $P^{(NHP)}$–M distances (2.2424(13) Å (**5**); 2.2446(11) Å (**9**)), similar to those in **3** and **4**.

Treatment of the (PPP)Pd-X complexes with $TlPF_6$ at room temperature generates the halide-abstraction products, dimers $[(PPP)Pd]_2[PF_6]_2$ (**1**) and $[(PPP)Pt]_2[PF_6]_2$ (**11**), as shown in Scheme 2. Complex **11** is isostructural to complex **1** and, thus, the NHP units in complex **11** feature bridging NHP^+ phosphenium character in agreement with the NHP^+/M^0 assignment (see Supporting Information). In analogy to the aforementioned reactivity of **1**, Pt dimer **11** reacts with PMe_3 to cleanly generate the NHP^- phosphido Pt^{II} complex $[(PPP)Pt(PMe_3)][PF_6]_2$ (**4**). Pd monomer $[(PPP)Pd(PMe_3)][PF_6]_2$ (**2**) can also be generated via addition of $TlPF_6$ to **5**–**7** in the presence of PMe_3.

Platinum complexes **8**–**10** are very unstable, especially in moderately polar solvents such as tetrahydrofuran (THF) or CH_2Cl_2. THF solutions of **8**–**10** decompose slowly at room temperature to generate unusual trinuclear Pt complexes **12**–**14** (Scheme 2). In contrast to **8**–**10**, ^{31}P NMR spectra of **12**–**14** feature a more upfield shift for the central NHP phosphorus atom (152.9 (**12**), 154.9 (**13**), 162.9 (**14**) ppm). In addition, hydride signals with coupling to both ^{31}P and ^{195}Pt can be detected in ^1H NMR spectra of **12**–**14** (−17.1(**12**), −16.2 (**13**), −13.3 (**14**) ppm). Consistent with the NMR spectral data, the solid state structures of **13** and **14** reveal that in these decomposition products two (PPP)Pt-X units are bridged symmetrically through a Pt(H)(X) fragment (Figure 3, Supporting Information). In contrast to complexes **1** and **11**, the NHPs in **13** and **14** are bridging NHP^- phosphide ligands acting as X-type donors to the flanking Pt centers and L-type donors to the central Pt center. Each of the three Pt centers is rigorously square planar, agreeing with this assignment of three Pt^{II} centers. The mechanism of decomposition to form **12**–**14** is unknown, but the products of prolonged exposure of **8**–**10** in deuterated dichloromethane do not exhibit hydride resonances by ^1H NMR, suggesting that solvent is origin of the hydrides in **12**–**14**.

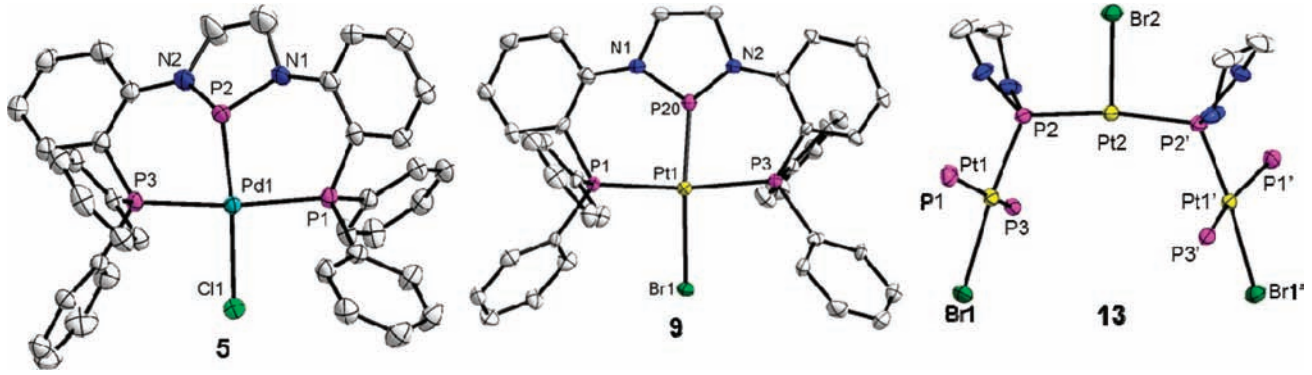

Figure 3. Displacement ellipsoid (50%) representation of **5**, **9**, and **13**. For clarity, all hydrogen atoms and solvate molecules have been omitted. In the case of **13**, aryl rings have also been omitted to reveal the core structure. The Pt-hydride ligand in **13** was not located crystallographically, and its position, therefore, is geometrically inferred. Relevant interatomic distances (Å) and angles (deg): **5:** P2–Pd, 2.2424(13); P1–Pd, 2.3151(11); P3–Pd, 2.3098(11); Cl1–Pd, 2.4530(11); P1–Pd–P2, 90.528(48); P2–Pd–P3, 81.563(48); P1–Pd–Cl1, 94.035(42); P3–Pd–Cl1, 93.020(42); P1–Pd–P3, 170.959(38); P3–Pd–Cl1, 169.080(51). **9:** P2–Pt, 2.2446(11); P1–Pt, 2.2901(19); P3–Pt, 2.2931(19); Br1–Pt, 2.5430(3); N1–Pt–N2, 89.055(168); P1–Pt–P2, 83.197(45); P2–Pt–P3, 90.224(45); P1–Pt–Br1, 93.856(31); P3–Pt–Br1, 93.434(30); P1–Pt–P3, 172.561(50); P2–Pt–Br1, 163.726(28). **13:** P2–Pt1, 2.2111(11); P2–Pt2, 2.2756(11); P1–Pt1, 2.2903(13); P3–Pt1, 2.2906(11), Br1–Pt1, 2.5341(4); Br2–Pt2, 2.5432(7); P1–Pt1–P2, 88.822(44); P2–Pt1–P3, 88.774(41); P1–Pt1–Br1, 94.200(32); P3–Pt1–Br1, 89.599(27); P1–Pt1–P3, 163.935(42); P2–Pt1–Br1, 174.398(29); P2–Pt2–Br2, 94.352(25).

dx.doi.org/10.1021/ic202581v | *Inorg. Chem.* 2012, 51, 4170–4179

Reactivity toward Small Molecule Activation. The noninnocent nature of NHP ligands in transition metal complexes suggests the ability to activate σ bonds across the $P^{(NHP)}$–M bond. Indeed, treatment of complexes **2**, **3**, or **4** with MeI results in the M^{II} iodide complexes $[(PP^{Me}P)MI][PF_6]$ (M = Pd (**15**), Pt (**17**)) and $[(PP^{Me}P)MI_2]$ (M = Pd (**16**), Pt (**18**), Scheme 3). The methyl group electrophilically attacks the

Scheme 3

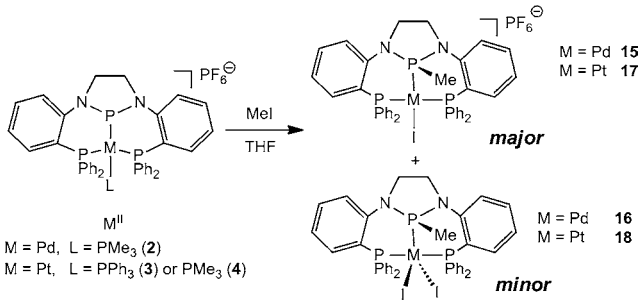

stereochemically active lone pair at the central NHP phosphorus to generate a trisubstituted phosphine ligand (L-type), providing further evidence for an electron-rich NHP^- phosphide ligand. In a formal sense, MeI has added to **2**, **3**, or **4** without altering the oxidation state of the metal center, which illustrates the noninnocent behavior of the NHP unit in these transition metal complexes.

While the anionic complexes **15** and **17** are the major products of these MeI addition reactions, appreciable quantities of the neutral diiodide complexes **16** and **18** are detected. The likely mechanism by which these byproducts are obtained involves attack of MeI on dissociated PPh_3 to generate $[PR_3Me]^+[I]^-$, which can then undergo anion exchange with either the starting material **2**–**4** or the MeI addition products **15** or **17** to generate neutral diiodide complexes **16** and **18** (see Supporting Information). The proposed intermediate $[PR_3Me]^+[I]^-$ was synthesized independently, and its presence confirmed in the MeI reaction mixture by ^1H and ^{31}P NMR spectroscopy. Alternatively, diiodide complexes **16** and **18** can be synthesized exclusively in >80% yields by adding excess phosphine ligand (PPh_3 or PMe_3) into the reaction of **2**–**4** and MeI.

The solid state structures of **17** and **16**, shown in Figure 4, reveal that the square planar geometry at the Pt and Pd center, respectively, have been maintained upon MeI addition across the M–$P^{(NHP)}$ bond. Methylation at the NHP phosphorus has a negligible effect on the M–$P^{(NHP)}$ distance in both cases, consistent with the maintenance of a M–P single bond. The second iodide ligand in **16** is bound weakly (Pd–I2 = 3.1464(2) Å) in an apical position, causing only a minor perturbation in the square planar geometry at Pd.

Theoretical Investigation of Group 10 NHP-diphosphine Complexes. To better understand the electronic structure of Pt and Pd complexes featuring the $[PPP]^+$ NHP-diphosphine pincer ligand, a computational investigation was carried out using density functional theory (DFT, B3LYP/LANL2DZ). Three Pt complexes were chosen for this study, $[(PPP)Pt(PMe_3)]^+$ (**4**), (PPP)PtI (**10**), and the three-coordinate complex (PPP)Pt (**11***), meant to represent half of dimer **11**. A geometry optimization and subsequent NBO calculation were performed on each complex starting from crystallographic coordinates. The Pt–P natural bond orbitals

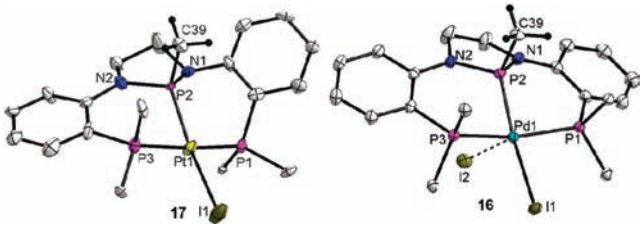

Figure 4. Displacement ellipsoid (50%) representation of **16** and **17**. For clarity, all hydrogen atom with the exception of those on the NHP-bound Me group have been omitted. Solvate molecules and PF_6^- counterions (**17**) have also been omitted. Relevant interatomic distances (Å) and angles (deg): **17**: P2–Pt, 2.228(3); Pt–P3, 2.311(4); Pt–P1, 2.322(4); P2–C39, 1.810(12); Pt–I1, 2.5961(8); I1–Pt–P2, 170.07(10); P3–Pt–P1, 173.45(11); Pt–P2–C39, 117.1(4). **16**: P2–Pd, 2.1984(5); Pd–P3, 2.3079(6); Pd–P1, 2.3051(6); P2–C39, 1.800(2); Pd–I1, 2.6617(2); Pd–I2, 3.1464(2); I1–Pd–P2, 170.590(16); P3–Pd–P1, 163.11(2); I1–Pd–I2, 105.726(7); Pd–P2–C39, 114.16(8).

for complexes **4** and **10** are covalent in nature with similar constitution, 41.6% Pt/58.4% P and 41.7% Pt/58.3% P character, respectively. In contrast, the Pt–P bonding in the three-coordinate complex **11*** is composed entirely of a strong donor–acceptor interaction (stabilization energy (E^{del}) = 111 kcal/mol) between the electron-rich Pt center and the empty p orbital on the central NHP phosphorus (Figure 5). This difference in bonding results from the absence of an additional two-electron donor ligand to stabilize a higher formal oxidation state at Pt in **11***. This data is consistent with the assignment of **4** and **10** as Pt^{II}/NHP^- phosphido complexes. In the absence of an additional donor ligand, **11*** is better assigned as a Pt^0/NHP^+ phosphenium complex in which the NHP is bound via a Pt-to-P donor–acceptor interaction.

The hypothetical two-electron oxidation products $\mathbf{4}^{ox}$, $\mathbf{10}^{ox}$, and $\mathbf{11}^{*ox}$ were also calculated using DFT and NBO analysis. Interestingly, upon optimization the geometry about the NHP unit in complexes $\mathbf{4}^{ox}$ and $\mathbf{10}^{ox}$ became more planar, although steric factors prevented a rigorously planar geometry in the PMe_3 complex $\mathbf{4}^{ox}$. The natural charge on the NHP phosphorus atom increases substantially upon oxidation of these two complexes, from 1.07 to 1.56 in $\mathbf{4}/\mathbf{4}^{ox}$ and from 1.01 to 1.65 in $\mathbf{10}/\mathbf{10}^{ox}$. In contrast, however, the natural charge on Pt increases only slightly in $\mathbf{4}/\mathbf{4}^{ox}$ (−0.58 to −0.43) and decreases in the case of $\mathbf{10}/\mathbf{10}^{ox}$ (−0.46 to −0.65). NBO analysis of $\mathbf{10}^{ox}$ reveals a Pt–P NBO that is strongly polarized toward phosphorus (71.2% P, 28.8% Pt), indicative of dative donation of the phosphorus lone pair to the divalent Pt center (Figure 5). The Pt–P interaction is further strengthened by a Pt→P π donor–acceptor interaction (E^{del} = 18.8 kcal/mol) between a filled Pt d orbital and the empty p orbital on the central NHP phosphorus atom. Because of the more electron-rich Pt center in $\mathbf{4}^{ox}$, an NBO corresponding to lone pair donation from the NHP phosphorus to Pt was not detected. The reduced symmetry in this distorted complex leads to less orbital overlap and weakening of the Pt→P π donor–acceptor interaction (E^{del} = 12.2 kcal/mol). Thus, *two-electron oxidation is predicted to lead to oxidation of the NHP phosphorus center to generate a phosphenium complex, with no change in formal oxidation state at Pt.* Notably, solution electrochemistry of both the phosphine adduct **3** and the Pt–Cl species **8** (analogues of **4** and **10**, respectively), reveals irreversible oxidation events at relatively mild potentials (−0.22 V for **3** and −0.24 V for **4**, see

dx.doi.org/10.1021/ic202581v | Inorg. Chem. 2012, 51, 4170–4179

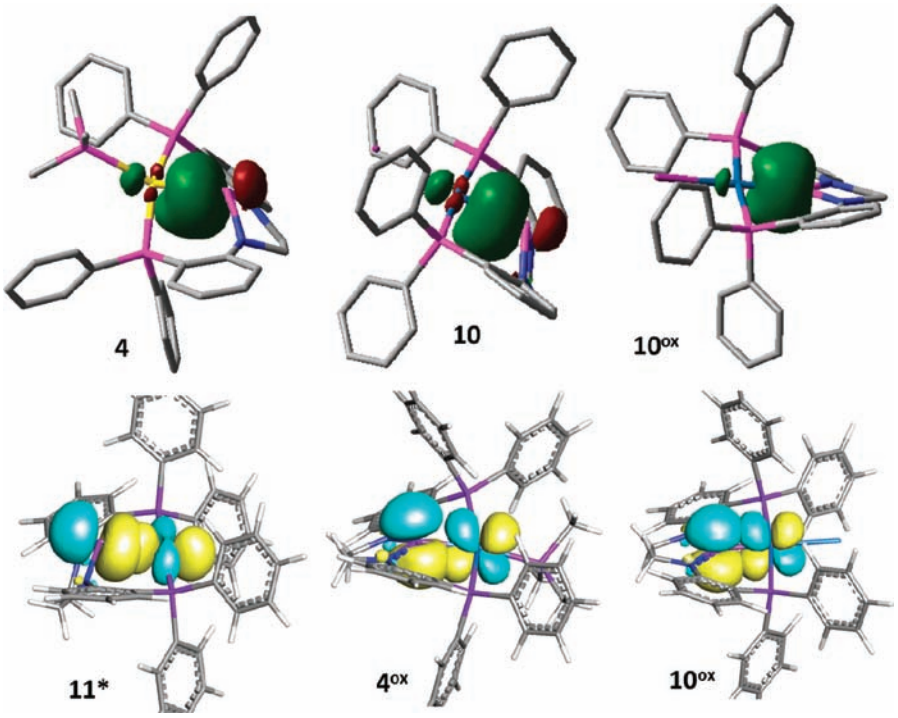

Figure 5. Visual representations of the calculated Pt−P NBOs of complex **4** (41.6% Pt, 58.4% P), **10** (41.7% Pt, 58.3% P), and **10**^{ox} (28.8% Pt, 71.2% P) (top). Pt to P donor−acceptor interactions in **11*** (E^{del}= 111 kcal/mol), **4**^{ox} (E^{del} = 12.2 kcal/mol), and **10**^{ox} (E^{del} = 18.8 kcal/mol) (bottom).

Supporting Information), suggesting that chemical oxidation of these complexes is possible but may not lead to stable products. In the case of the three-coordinate complex **11***^{ox}, oxidation appears to be Pt-centered, with a large increase in natural charge at Pt (−0.32 to 0.03) and small change in the natural charge at the NHP phosphorus atom (1.25 to 1.48), since the NHP unit is already in the oxidized NHP$^+$ phosphenium state in **11***.

Wiberg bond indices (WBIs) for all six complexes were also calculated and are tabulated in Table 1. All six N−C WBI values

Table 1. Calculated Wiberg Bond Indices (WBIs) for Complexes 4, 10, 11*, 4^{ox}**, 10**^{ox}**, and 11***^{ox}

	P−Pt	P−N	N−C
4	0.84	0.74	0.93
10	0.80	0.72	0.93
11*	0.80	0.81	0.92
4^{ox}	0.73	1.01	0.90
10^{ox}	0.95	0.99	0.91
11*^{ox}	0.88	0.96	0.90

are shown to depict that a typical single bond is represented by a WBI of about 0.91. Notably, as each compound is oxidized a substantial increase in the P−N WBI is observed, implying stronger donation from the nitrogen lone pairs to the central NHP phosphorus atom as it gains NHP$^+$ phosphenium character. A corresponding increase in P−Pt WBI is also observed upon oxidation in the cases of complexes **10**^{ox} and **11***^{ox}, consistent with both σ and π interactions between P and Pt. The Pt−P WBI decreases upon oxidation of **4** to **4**^{ox}, likely the result of steric constraints restricting orbital overlap.

CONCLUSION

In summary, incorporation of an NHP unit into a chelating bis(phosphine) framework has allowed a systematic investigation of NHP coordination chemistry at Pd and Pt. We have established that in the case of electron-rich metal fragments (e.g., group 10 metal with 3 additional L-type donors), the pyramidal geometry adopted by the central NHP donor ligand is attributed to a NHP$^-$ phosphido description accompanied by formal two-electron oxidation of the metal center. Indeed, cyclic voltammetry (CV) of the free phosphenium ligand [PPP][PF_6] reveals multielectron reduction events at reasonably mild potentials (−1.6 to −1.8 V vs ferrocene, see Supporting Information), consistent with the observation that two-electron transfer can occur upon treatment with reasonably electron-rich d^{10} metal precursors. NHPs bound to metal fragments with fewer electrons (e.g., group 10 metal with only 2 additional L-type donors), however, maintain phosphenium character and adopt the canonical planar NHP$^+$ geometry. We have also shown that interconversion between these two geometries can be affected by either coordination/dissociation of a two-electron donor ligand or two-electron redox processes.

Several key points bear further mention:

(1) Herein we have discussed transition metal complexes of both NHP$^+$ and NHP$^-$ ligands and it is noteworthy that we have elucidated a trend by which these two limiting descriptions can be differentiated via ^{31}P NMR. In our work, NHP$^-$ phosphenium complexes have ^{31}P NMR shifts lower than 250 ppm, while bona fide NHP$^+$ phosphenium complexes have shifts downfield of 250 ppm. We note, however, that while this trend in ^{31}P shift is useful for this particular chelating NHP-diphosphine ligand, previously reported complexes of Pt and Pd with monodentate NHP ligands (only NHP$^+$ phosphenium

dx.doi.org/10.1021/ic202581v | Inorg. Chem. 2012, 51, 4170−4179

complexes have been described) have chemical shifts that vary considerably with ancillary ligands.[21,23,24] In the case of Pt-NHP complexes, however, NHP^- and NHP^+ binding modes can easily be distinguished in all cases by $^1J_{Pt-P}$, as phosphenium ligands are bound more tightly to Pt through both σ and π interactions, leading to larger coupling constants (>2000 Hz).

(2) It is worthy of mention that previously reported Group 10 NHP complexes have, without exception, featured planar NHP^+ geometries indicative of a phosphenium cation bound to a low valent metal center.[21,23,24] Thus, a question arises as to why incorporation into a chelating framework would impart such a drastic change on metal binding preferences. One might argue that the (NHP)-ML_2 (L = NHC or phosphine) complexes reported in the literature maintain a planar phosphenium geometry as a result of the absence of a third L-type ligand, similar to the dimeric complexes **1** and **11**.[23,24] However, the $(NHP)M(PMe_3)_3$ complexes of Jones and co-workers are also reported to be NHP^+ phosphenium complexes based on ^{31}P NMR data (large $^1J_{Pt-P}$ and equivalence of PMe_3 ligands suggest a tetrahedral metal geometry).[23] The clearest difference between the $[(PPP)M\text{-}L]^+$ complexes reported herein and the aforementioned four-coordinate complexes is the planar geometry enforced by the chelating nature of the $[PPP]^+$ ligand. NHP (and NHC) ligands with N-aryl substitutents typically adopt a geometry in which the aryl group orients perpendicular to the plane of the heterocycle, but in the case of a pincer ligand, these aryl groups are forced to orient in the same plane as the heterocycle. As a consequence, it seems feasible that the lone pair of electrons on the nitrogen atoms can delocalize throughout the appended aromatic rings in the latter case, withdrawing electron density that would otherwise be involved in donation to the empty orbital on the central phosphorus to stabilize the cationic phosphenium center (Chart 2). A consequence of this phenomenon would be relative stabilization of the triplet state of the NHP, thus favoring the anionic phosphide binding mode. Moreover, NHPs with pendant coplanar aryl rings that continue to adopt a planar NHP^+ binding mode would be expected to be stronger π-acceptors. This principle may, in fact, hold true for *all* pincer ligands containing both NHPs *and* NHCs.

Chart 2

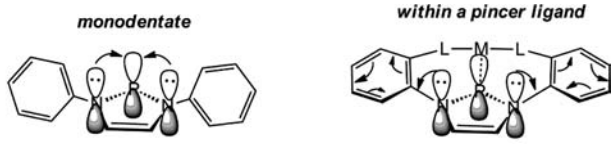

The strong analogy between NHPs and nitrosyls has been substantiated by this study, revealing both electronic and structural (in terms of dual binding modes) similarities. For this reason, NHPs have great potential as sterically and electronically tunable noninnocent ligands in coordination chemistry and catalysis. Moreover, incorporation of NHPs into a chelating framework provides a method to impart stability to transition metal NHP complexes in various redox states. Future studies will continue to focus on the coordination chemistry of NHP-diphosphine ligands and their derivatives.

EXPERIMENTAL SECTION

General Considerations. All syntheses reported were carried out using standard glovebox and Schlenk techniques in the absence of water and dioxygen, unless otherwise noted. Benzene, *n*-pentane, tetrahydrofuran, toluene, diethyl ether, and dichloromethane were degassed and dried by sparging with ultra high purity argon gas followed by passage through a series of drying columns using a Seca Solvent System by Glass Contour. All solvents were stored over 3-Å molecular sieves. Deuterated solvents were purchased from Cambridge Isotope Laboratories, Inc., degassed via repeated freeze−pump−thaw cycles, and dried over 3-Å molecular sieves. Solvents were frequently tested using a standard solution of sodium benzophenone ketyl in tetrahydrofuran to confirm the absence of oxygen and moisture. Ligand precursor [PPP]-X,[19] ligand $[PPP][PF_6]$,[19] $Pd(PPh_3)_4$,[29] and $Pt(PPh_3)_4$[30] were synthesized using literature procedures. Methyl iodide, triphenylphosphine, and trimethylphosphine were purchased from commercial vendors and used without further purification. NMR spectra were recorded at ambient temperature unless otherwise stated on Varian Inova 400 MHz instrument. ^1H and ^{13}C NMR chemical shifts were referenced to residual solvent and are reported in ppm. ^{31}P NMR chemical shifts (in ppm) were referenced to 85% H_3PO_4 (0 ppm). ^{19}F NMR chemical shifts (in ppm) were referenced to 1% trifluoroacetic acid (−76.5 ppm). Elemental microanalyses were performed by Complete Analysis Laboratories, Inc., Parsippany, NJ.

$[(PPP)Pd]_2[PF_6]_2$ (1). Ligand $[PPP][PF_6]$ (105 mg, 0.145 mmol) was suspended in 10 mL of THF; to this yellow suspension was added $Pd(PPh_3)_4$ (161 mg, 0.139 mmol). The mixture became dark brown within 5 min but was allowed to stir at room temperature (rt) further to ensure completion. After 1 h, volatiles were removed from the resulting solution in vacuo, and the resulting brown residue was washed with diethyl ether (3 × 5 mL). Crystallization of the crude brown product via vapor diffusion of diethyl ether into a concentrated THF solution resulted in analytically pure product as dark red crystals suitable for X-ray diffraction (73.1 mg, 60.8%). ^1H NMR (400 MHz, CD_2Cl_2): δ 7.61 (m, 12H, Ar-*H*), 7.55 (m, 4H, Ar-*H*), 7.47 (t, 8H, Ar-*H*), 7.32 (m, 4H, Ar-*H*), 7.26 (m, 8H, Ar-*H*), 7.05 (t, 4H, Ar-*H*), 6.86 (br, 12H, Ar-*H*), 6.56 (br, 4H, Ar-*H*), 3.36 (m, 4H, CH_2), 3.05 (m, 4H, CH_2). ^{31}P NMR (161.8 MHz, CD_2Cl_2): δ 288.3 (br s, 2P), 14.1 (br s, 4P), −143.8 (sept, 1P, $^1J_{P-F}$ = 710 Hz). ^{13}C NMR (100.5 MHz, CD_2Cl_2): δ 133.9, 133.2, 132.6, 132.2, 129.7, 129.6, 129.5, 126.9, 120.0. 118.9, 51.2. Anal. Calcd. for $C_{76}H_{64}N_4F_{12}P_8Pd_2$: C, 53.01; H, 3.75; N, 3.25. Found: C, 53.03; H, 3.68; N, 3.26.

$[(PPP)Pd(PMe_3)][PF_6]$ (2). Compound **1** (35.0 mg, 0.0203 mmol) was dissolved in 10 mL of CH_2Cl_2 and to this dark red solution was added trimethylphosphine (8.4 μL, 0.081 mmol). The mixture was allowed to stir for 12 h to ensure complete reaction. Subsequent removal of the volatiles from the resulting brown solution yielded analytically pure product as a yellow solid (35.1 mg, 92.2%). Crystals suitable for X-ray crystallography were grown via slow evaporation of a concentrated THF solution of the product in the freezer (−35 °C). ^1H NMR (400 MHz, CD_2Cl_2): δ 7.53 (m, 14H, Ar-*H*), 7.35 (m, 8H, Ar-*H*), 7.26 (m, 2H, Ar-*H*), 7.22 (m, 2H, Ar-*H*), 7.06 (t, 2H, Ar-*H*), 3.79 (m, 2H, CH_2), 3.06 (m, 2H, CH_2), 0.57 (d, 9H, $-CH_3$, $^2J_{P-H}$ = 6.8 Hz). ^{31}P NMR (161.8 MHz, CD_2Cl_2): δ 235.6 (t, 1P, $^2J_{P-P}$ = 24.3 Hz), 11.5 (dd, 2P, $^2J_{P-P}$ = 24.3 Hz, $^2J_{P-P}$ = 57.0 Hz), −34.1 (t, 1P, $^2J_{P-P}$ = 57.0 Hz), −143.9 (sept, 1P, $^1J_{P-F}$ = 710 Hz). ^{13}C NMR (100.5 MHz, CD_2Cl_2): δ 134.6, 134.5, 134.0, 132.4, 131.9, 131.7, 129.6, 129.5, 122.1, 121.0, 50.2, 21.4. Anal. Calcd for $C_{41}H_{41}N_2F_6P_5Pd$: C, 52.55; H, 4.41; N, 2.99. Found: C, 52.64; H, 4.57; N, 3.89.

$[(PPP)Pt(PPh_3)][PF_6]$ (3). Ligand $[PPP][PF_6]$ (92.0 mg, 0.122 mmol) was suspended in 10 mL of THF and to this yellow suspension was added $Pt(PPh_3)_4$ (152 mg, 0.122 mmol). The resulting mixture was allowed to stir at rt further to ensure complete reaction. After 1 h, volatiles were removed from the red solution in vacuo, and the remaining residue was washed with diethyl ether (3 × 5 mL). Crystallization of the crude product via vapor diffusion of diethyl ether

dx.doi.org/10.1021/ic202581v | *Inorg. Chem.* 2012, 51, 4170−4179

into a concentrated THF solution resulted in product as red crystals suitable for X-ray diffraction (115 mg, 77.8%). ^{1}H NMR (400 MHz, $CDCl_3$): δ 7.56 (t, 2H, Ar-*H*), 7.54 (t, 2H, Ar-*H*), 7.38 (t, 4H, Ar-*H*), 7.32−6.89 (m, 31H, Ar-*H*), 6.26 (m, 4H, Ar-*H*), 3.76 (br, 2H, CH_2), 2.67 (br, 2H, CH_2). ^{31}P NMR (161.8 MHz, $CDCl_3$): δ 198.8 (ddt, 1P, $^1J_{Pt-P}$ = 445 Hz, $^2J_{P-P(trans)}$ = 52.1 Hz, $^2J_{P-P(cis)}$ = 9.2 Hz), 29.1 (ddt, 1P, $^1J_{Pt-P}$ = 2443 Hz, $^2J_{P-P(trans)}$ = 52.1 Hz, $^2J_{P-P(cis)}$ = 22.0 Hz), 13.6 (ddd, 2P, $^1J_{Pt-P}$ = 3446 Hz, $^2J_{P-P(NHP)}$ = 9.2 Hz, $^2J_{P-(PPh3)}$ = 22.0 Hz), −143.9 (sept, 1P, $^1J_{P-F}$ = 710 Hz). ^{13}C NMR (100.5 MHz, $CDCl_3$): δ 146.7, 134.6, 134.5, 134.1, 134.0, 132.7, 132.3, 132.1, 131.5, 131.3, 128.9, 128.8, 121.8, 119.2, 48.2. Anal. Calcd for $C_{56}H_{47}N_2F_6P_5Pt$: C, 55.60; H, 3.91; N, 2.31. Found: C, 55.45; H, 4.01; N, 2.26.

[(PPP)Pt(PMe$_3$)][PF$_6$] (4). Compound **3** (31.8 mg, 0.0262 mmol) was dissolved in 10 mL of dichloromethane and to this red solution was added trimethylphosphine (5.4 μL, 0.052 mmol). The reaction mixture was allowed to stir further to ensure complete reaction. After 1 h, removal of all volatiles from the resulting yellow solution yielded analytically pure product as yellow solid (25.7 mg, 95.6%). Crystals suitable for X-ray crystallography were grown via vapor diffusion of *n*-pentane into a concentrated dichloromethane solution of **4**. ^{1}H NMR (400 MHz, $CDCl_3$): δ 7.47 (m, 12H, Ar-*H*), 7.27 (m, 8H, Ar-*H*), 7.16 (m, 2H, Ar-*H*), 6.96 (m, 4H, Ar-*H*), 6.82 (t, 2H, Ar-*H*), 3.58 (m, 2H, CH_2), 3.18 (m, 2H, CH_2), 0.65 (d, 9H, CH_3). ^{31}P NMR (161.8 MHz, $CDCl_3$): δ 205.5 (ddt, 1P, $^1J_{Pt-P}$ = 496 Hz, $^2J_{P-P(trans)}$ = 54.9 Hz, $^2J_{P-P(cis)}$ = 9.1 Hz), 11.1 (ddd, 2P, $^1J_{Pt-P}$ = 3149 Hz, $^2J_{P-P(NHP)}$ = 9.1 Hz, $^2J_{P-PMe3}$ = 26.5 Hz), −18.7 (ddt, 1P, $^1J_{Pt-P}$ = 2221 Hz, $^2J_{P-P(NHP)}$ = 54.9 Hz, $^2J_{P-(cis)}$ = 26.5 Hz), −143.9 (sept, 1P, $^1J_{P-F}$ = 710 Hz). ^{13}C NMR (100.5 MHz, $CDCl_3$): δ 134.7, 134.6, 134.4, 132.3, 132.0, 131.8, 129.7, 129.6, 121.5, 121.1, 49.5, 20.8. Anal. Calcd for $C_{41}H_{41}N_2F_6P_5Pt$: C, 48.01; H, 4.03; N, 2.73. Found: C, 47.83; H, 4.02; N, 2.63.

(PPP)Pd−Cl (5). Ligand precursor [PPP]-Cl (128 mg, 0.198 mmol) was dissolved in 10 mL of benzene; to this stirring pale yellow solution was added $Pd(PPh_3)_4$ (229 mg, 0.198 mmol). The reaction mixture became dark red immediately, and after 5 min, the dark red solution was filtered and concentrated to about 2 mL. Upon standing for 12 h at rt, yellow crystals formed and were washed with benzene and further dried in vacuo to yield pure product (79.7 mg, 49.4%). ^{1}H NMR (400 MHz, CD_2Cl_2): δ 7.68 (m, 4H, Ar-*H*), 7.52 (m, 4H, Ar-*H*), 7.48−7.41 (m, 10H, Ar-*H*), 7.36 (m, 4H, Ar-*H*), 7.19 (m, 2H, Ar-*H*), 6.97 (m, 2H, Ar-*H*), 6.88 (t, 2H, Ar-*H*), 3.83 (m, 2H, CH_2), 3.36 (m, 2H, CH_2). ^{31}P NMR (161.8 MHz, CD_2Cl_2): δ 248.6 (t, $^1J_{P-P}$ = 28.3 Hz), 6.2 (d, $^1J_{P-P}$ = 28.3 Hz). ^{13}C NMR (100.5 MHz, CD_2Cl_2): δ 136.1, 134.8, 134.3, 131.8, 130.5, 130.4, 128.5, 128.4, 121.7, 121.2, 51.6.Anal. Calcd for $C_{38}H_{32}N_2ClP_3Pd$: C, 60.74; H, 4.29; N, 3.73. Found: C, 60.58; H, 4.37; N, 3.59.

(PPP)Pd−Br (6). An identical procedure to that of compound **5** was followed, using [PPP]-Br (53.7 mg, 0.078 mmol) and $Pd(PPh_3)_4$ (90.0 mg, 0.078 mmol) to yield **6** (40.0 mg, 64.5%). ^{1}H NMR (400 MHz, CD_2Cl_2): δ 7.68 (m, 4H, Ar-*H*), 7.53 (m, 4H, Ar-*H*), 7.51−7.43 (m, 10H, Ar-*H*), 7.37 (m, 4H, Ar-*H*), 7.21 (m, 2H, Ar-*H*), 6.98 (m, 2H, Ar-*H*), 6.89 (t, 2H, Ar-*H*), 3.84(m, 2H, CH_2), 3.36 (m, 2H, CH_2). ^{31}P NMR (161.8 MHz, CD_2Cl_2): δ 246.1 (t, $^1J_{P-P}$ = 25.2 Hz), 6.0 (d, $^1J_{P-P}$ = 25.2 Hz). ^{13}C NMR (100.5 MHz, CD_2Cl_2): δ 136.3, 134.7, 134.4, 131.8, 130.5, 130.4, 128.4, 128.3, 121.9, 121.4, 51.9. Repeated attempts to obtain satisfactory combustion analysis data for **6** were unsuccesful as a result of an unidentified minor impurity that cocrystallized with **6**.

(PPP)Pd−I (7). An identical procedure to that of compound **5** was followed, using [PPP]-I (46.6 mg, 0.063 mmol) and $Pd(PPh_3)_4$ (73.1 mg, 0.063 mmol) to yield **7** (23.3 mg, 43.7%). ^{1}H NMR (400 MHz, CD_2Cl_2): δ 7.69 (m, 4H, Ar-*H*), 7.52 (m, 4H, Ar-*H*), 7.48−7.43 (m, 10H, Ar-*H*), 7.36 (m, 4H, Ar-*H*), 7.21 (m, 2H, Ar-*H*), 6.98 (m, 2H, Ar-*H*), 6.86 (t, 2H, Ar-*H*), 3.83(m, 2H, CH_2), 3.35 (m, 2H, CH_2). ^{31}P NMR (161.8 MHz, CD_2Cl_2): δ 242.2 (t, $^1J_{P-P}$ = 25.0 Hz), 5.7 (d, $^1J_{P-P}$ = 25.0 Hz) ^{13}C NMR (100.5 MHz, $CDCl_3$): δ 136.1, 134.9, 134.4, 131.7, 130.4, 130.3, 128.5, 128.2, 121.9, 121.3, 52.0. Anal. Calcd for $C_{38}H_{32}N_2IP_3Pd$: C, 54.15; H, 3.83; N, 3.32. Found: C, 54.26; H, 3.89; N, 3.34.

(PPP)Pt−Cl (8). Ligand precusor [PPP]-Cl (97.0 mg, 0.150 mmol) was dissolved in 10 mL of toluene and to this stirring light yellow solution was added $Pt(PPh_3)_4$ (187 mg, 0.150 mmol). The reaction mixture became deep red immediately. After stirring for 10 min, the resulting red solution was filtered and concentrated in vacuo to about 5 mL. The concentrated toluene solution was stored in the freezer for 12 h (−35 °C), affording **8** as yellow crystals which were collected, washed with toluene, and further dried in vacuo (98.0 mg, 77.6%). ^{1}H NMR (400 MHz, CD_2Cl_2): δ 7.68 (m, 4H, Ar-*H*), 7.47 (m, 10H, Ar-*H*), 7.37 (m, 8H, Ar-*H*), 7.05 (d, 2H, Ar-*H*), 6.86 (q, 2H, Ar-*H*), 6.74 (t, 2H, Ar-*H*), 3.76(m, 2H, CH_2), 3.38 (m, 2H, CH_2). ^{31}P NMR (161.8 MHz, CD_2Cl_2): δ 224.8 (dt, $^1J_{Pt-P}$ = 663 Hz, $^1J_{P-P}$ = 6.1 Hz), 12.1 (dd, $^1J_{Pt-P}$ = 3304 Hz, $^1J_{P-P}$ = 6.1 Hz). ^{13}C NMR (100.5 MHz, CD_2Cl_2): δ 135.9, 134.8, 134.2, 132.2, 130.8 130.7, 128.3, 128.2, 119.2, 118.6, 48.6. Anal. Calcd for $C_{38}H_{32}N_2ClP_3Pt$: C, 54.33; H, 3.84; N, 3.33. Found: C, 54.28; H, 3.91; N, 3.16.

(PPP)Pt−Br (9). An identical procedure to that of compound **8** was followed, using [PPP]-Br (84.5 mg, 0.123 mmol) and $Pt(PPh_3)_4$ (152.5 mg, 0.123 mmol) to yield **9** (76.5 mg, 70.6%). ^{1}H NMR (400 MHz, CD_2Cl_2): δ 7.67 (m, 4H, Ar-*H*), 7.46−7.34 (m, 18H, Ar-*H*), 7.06 (m, 2H, Ar-*H*), 6.85 (q, 2H, Ar-*H*), 6.74 (t, 2H, Ar-*H*), 3.77(m, 2H, CH_2), 3.34 (m, 2H, CH_2). ^{31}P NMR (161.8 MHz, CD_2Cl_2): δ 222.0 (dt, $^1J_{Pt-P}$ = 607 Hz, $^1J_{P-P}$ = 6.1 Hz), 11.2 (dd, $^1J_{Pt-P}$ = 3337 Hz, $^1J_{P-P}$ = 6.1 Hz). ^{13}C NMR (100.5 MHz, CD_2Cl_2): 136.1, 134.8, 134.3, 132.1, 130.8 130.7, 128.4, 128.2, 119.4, 119.0, 48.8. Anal. Calcd for $C_{38}H_{32}N_2BrP_3Pt$: C, 51.60; H, 3.65; N, 3.17. Found: C, 51.43; H, 3.72; N, 3.08.

(PPP)Pt−I (10). An identical procedure to that of compound **8** was followed, using [PPP]-I (123.4 mg, 0.168 mmol) and $Pt(PPh_3)_4$ (208.5 mg, 0.168 mmol) to yield **10** (72.5 mg, 46.4%). ^{1}H NMR (400 MHz, CD_2Cl_2): δ 7.65 (m, 4H, Ar-*H*), 7.45−7.35 (m, 18H, Ar-*H*), 7.07 (m, 2H, Ar-*H*), 6.90 (m, 2H, Ar-*H*), 6.75 (t, 2H, Ar-*H*), 3.79 (m, 2H, CH_2), 3.29 (m, 2H, CH_2). ^{31}P NMR (161.8 MHz, CD_2Cl_2): δ 219.5 (dt, $^1J_{Pt-P}$ = 486 Hz, $^1J_{P-P}$ = 6.4 Hz), 9.4 (dd, $^1J_{Pt-P}$ = 3350 Hz, $^1J_{P-P}$ = 6.4 Hz). ^{13}C NMR (100.5 MHz, CD_2Cl_2): δ 136.3, 134.9, 134.4, 132.0, 130.6, 130.7, 128.4, 128.1, 119.5, 119.2, 48.9. Anal. Calcd for $C_{38}H_{32}N_2IP_3Pt$: C, 48.99; H, ; 3.46N, 3.01. Found: C, 48.83; H, 3.51; N, 2.94.

[(PPP)Pt]$_2$[PF$_6$]$_2$ (11). Compound **8** (47.4 mg, 0.0564 mmol) was dissolved in 10 mL of THF and to this yellow solution was added $TlPF_6$ (19.7 mg, 0.0564 mmol). The mixture was allowed to stir at rt for 12 h to ensure complete reaction, and the resulting red solution was filtered through a pad of Celite to remove TlCl. Removal of the volatiles from the filtrate in vacuo afforded the crude product as a dark solid. Crystallization of the crude product via vapor diffusion of diethyl ether into a concentrated THF solution yielded product as dark red crystals suitable for X-ray diffraction. ^{1}H NMR (400 MHz, CD_2Cl_2): δ 7.58 (m, 6H, Ar-*H*), 7.49 (m, 2H, Ar-*H*), 7.31 (m, 10H, Ar-*H*), 7.07 (m, 4H, Ar-*H*), 6.99 (t, 2H, Ar-*H*), 6.80 (br, 2H, Ar-*H*), 6.61 (br, 2H, Ar-*H*), 3.43 (m, 2H, CH_2), 3.06 (m, 2H, CH_2). ^{31}P NMR (161.8 MHz, CD_2Cl_2): δ 257.5 (dd, $^1J_{Pt-P}$ = 2161 Hz, $^2J_{P-P}$ = 42 Hz), 5.4 (br, $^2J_{P-P}$ = 42 Hz), −143.9 (sept, $^1J_{P-F}$ = 710 Hz). Attempts to obtain satisfactory ^{13}C NMR and combustion analysis data for **11** were unsuccesful as a result of an unidentified minor impurity that cocrystallized with **11**. For this reason, an isolated yield has also not been reported.

[(PPP)Pt−Cl]$_2$Pt(H)(Cl) (12). Compound **8** (67.7 mg, 0.0806 mmol) was loaded into a 20 mL vial and stirred in 10 mL of THF. The resulting yellow mixture was allowed to stir vigorously for 12 h, and the volatiles were subsequently removed to afford a yellow solid. Crystallization of the crude product via vapor diffusion of diethyl ether into a concentrated THF solution afforded analytically pure product as yellow crystals (23.2 mg, 45.2%). ^{1}H NMR (400 MHz, CD_2Cl_2): δ 7.51 (m, 16H, Ar-*H*), 7.38−7.23 (m, 28H, Ar-*H*), 6.79 (m, 4H, Ar-*H*), 6.71 (m, 4H, Ar-*H*), 6.60 (m, 4H, Ar-*H*), 3.62 (m, 4H, CH_2), 3.19 (m, 4H, CH_2), −17.1 (dt, 1H, Pt-*H*, $^1J_{Pt-H}$ = 1300 Hz, $^1J_{P-H}$ = 21 Hz). ^{31}P NMR (161.8 MHz, CD_2Cl_2): δ 152.9 ($^1J_{Pt-P(side\ Pt)}$ = 529 Hz, $^1J_{Pt-P(central\ Pt)}$ = 2377 Hz, $^2J_{P-P}$ = 30 Hz), 4.1 ($^1J_{Pt-P}$ = 2586 Hz, $^2J_{P-P}$ = 30 Hz). ^{13}C NMR (100.5 MHz, CD_2Cl_2): δ 150.5, 135.8, 135.0, 134.1, 132.4, 130.5, 128.3, 128.2, 119.4, 118.5, 47.0. Anal. Calcd for

dx.doi.org/10.1021/ic202581v | *Inorg. Chem.* 2012, 51, 4170−4179

$C_{76}H_{65}N_4Cl_3P_6Pt_3$: C, 47.75; H, 3.43; N, 2.93. Found: C, 47.80; H, 3.37; N, 2.89.

[(PPP)Pt−Br]$_2$Pt(H)(Br) (13). An identical procedure to that of compound **12** was followed, using **9** (54.7 mg, 0.0793 mmol) to yield **13** (19.7, 36.4%). ^{1}H NMR (400 MHz, CD_2Cl_2): δ 7.55 (m, 16H, Ar-*H*), 7.40−7.22 (m, 28H, Ar-*H*), 6.78 (m, 4H, Ar-*H*), 6.68 (m, 4H, Ar-*H*), 6.59 (m, 4H, Ar-*H*), 3.60 (m, 4H, C*H*$_2$), 5.15 (m, 4H, C*H*$_2$), −16.2 (dt, 1H, Pt-*H*, $^1J_{Pt-H}$ = 1425 Hz, $^1J_{P-H}$ = 17 Hz). ^{31}P NMR (161.8 MHz, CD_2Cl_2): δ 154.9 ($^1J_{Pt-P(side\ Pt)}$ = 660 Hz, $^1J_{Pt-P(central\ Pt)}$ = 2750 Hz, $^2J_{P-P}$ = 25 Hz), 4.1 ($^1J_{Pt-P}$ = 2586 Hz, $^2J_{P-P}$ = 25 Hz). ^{13}C NMR (100.5 MHz, CD_2Cl_2): δ 150.4, 135.8, 135.0, 134.2, 132.4, 130.4, 128.1, 128.0, 120.0, 119.1, 46.8. Anal. Calcd for $C_{76}H_{65}N_4Br_3P_6Pt_3$: C, 44.63; H, 3.20; N, 2.74. Found: C, 44.62; H, 3.10; N, 2.71.

[(PPP)Pt−I]$_2$Pt(H)(I) (14). An identical procedure to that of compound **12** was followed, using **10** (58.8 mg, 0.0798 mmol) to yield **14** (29.7 mg, 51.1%). ^{1}H NMR (400 MHz, CD_2Cl_2): δ 7.62 (m, 16H, Ar-*H*), 7.43−7.23 (m, 28H, Ar-*H*), 6.83 (m, 8H, Ar-*H*), 6.52 (m, 4H, Ar-*H*), 3.57 (m, 4H, C*H*$_2$), 2.95 (m, 4H, C*H*$_2$), −13.3 (dt, 1H, Pt-*H*, $^1J_{Pt-H}$ = 1487 Hz, $^1J_{P-H}$ = 12 Hz). ^{31}P NMR (161.8 MHz, CD_2Cl_2): δ 162.9 ($^1J_{Pt-P(side\ Pt)}$ = 681 Hz, $^1J_{Pt-P(central\ Pt)}$ = 2436 Hz), 0.1 ($^1J_{Pt-P}$ = 3048 Hz). ^{13}C NMR (100.5 MHz, CD_2Cl_2): δ 150.5, 135.5, 135.2, 134.8, 132.4, 130.5, 128.0, 127.9, 121.1, 119.7, 46.7. Anal. Calcd for $C_{76}H_{65}N_4Cl_3P_6Pt_3$: C, 41.75; H, 3.00; N, 2.56. Found: C, 41.68; H, 3.02; N, 2.59.

[(PP(Me)P)PdI][PF$_6$] (15). Compound **2** (62.6 mg, 0.0668 mmol) was dissolved in 10 mL of dichloromethane. To this yellow solution was added MeI (4.2 μL, 0.067 mmol) and the mixture was allowed to stir for 12 h to ensure complete reaction. Removal of the volatiles afforded the crude product as a yellow residue. Crystallization of the crude product via vapor diffusion of pentane into a concentrated CH_2Cl_2 solution yielded analytically pure product as yellow crystals (32.4 mg, 48.3%). ^{1}H NMR (400 MHz, CD_2Cl_2): δ 7.68 (t, 2H, Ar-*H*), 7.62 (m, 6H, Ar-*H*), 7.54 (m, 6H, Ar-*H*), 7.42 (m, 10H, Ar-*H*), 7.09 (t, 2H, Ar-*H*), 7.03 (t, 2H, Ar-*H*), 4.36 (m, 2H, C*H*$_2$), 3.67 (m, 2H, C*H*$_2$), 1.11 (d, 2H, C*H*$_3$). ^{31}P NMR (161.8 MHz, CD_2Cl_2): δ 108.2 (t, $^2J_{P-P}$ = 23.6 Hz), −1.3 (d, $^2J_{P-P}$ = 23.6 Hz), −143.9 (sept, 1P, $^1J_{P-F}$ = 710 Hz). ^{13}C NMR (100.5 MHz, CD_2Cl_2): δ 144.6, 137.5, 134.9, 134.2, 132.6, 132.0, 129.5, 129.0, 123.4, 120.5, 47.3, 20.7. Anal. Calcd for $C_{39}H_{35}N_2IF_6P_4Pd$: C, 46.71; H, 3.52; N, 2.79. Found: C, 46.76; H, 3.55; N, 2.80.

[(PP(Me)P)PdI$_2$] (16). Compound **2** (83.0 mg, 0.0886 mmol) was dissolved in 10 mL of dichloromethane. To this yellow solution was added PMe_3 (43.6 μL, 0.421 mmol) and MeI (5.2 μL, 0.084 mmol). The resulting mixture was allowed to stir for 12 h to ensure complete reaction and the volatiles were subsequently removed to afford crude product as a yellow solid. Crystallization of the crude product via vapor diffusion of pentane into a concentrated CH_2Cl_2 solution yielded analytically pure product as yellow crystals (90.0 mg, 83.1%). ^{1}H NMR (400 MHz, CD_2Cl_2): δ 7.64 (m, 6H, Ar-*H*), 7.57 (m, 2H, Ar-*H*), 7.49 (m, 12H, Ar-*H*), 7.42 (m, 4H, Ar-*H*), 7.05 (m, 4H, Ar-*H*), 4.57 (m, 2H, C*H*$_2$), 3.78 (m, 2H, C*H*$_2$), 1.14 (d, 2H, C*H*$_3$). ^{31}P NMR (161.8 MHz, CD_2Cl_2): δ 104.4 (t, $^2J_{P-P}$ = 21.2 Hz), −2.9 (d, $^2J_{P-P}$ = 21.2 Hz). ^{13}C NMR (100.5 MHz, CD_2Cl_2): δ 146.5, 137.5, 135.0, 134.2, 132.3, 131.7, 129.4, 128.8, 122.9, 120.7, 48.1, 19.9 Anal. Calcd for $C_{39}H_{35}N_2I_2P_3Pd$: C, 47.56; H, 3.58; N, 2.84. Found: C, 47.48; H, 3.57; N, 2.90.

[(PP(Me)P)PtI][PF$_6$] (17). Compound **3** (73.2 mg, 0.0604 mmol) was dissolved in 10 mL of THF and to this stirring red solution was added MeI (3.8 μL, 0.060 mmol). The mixture was stirred at rt for 12 h to ensure complete reaction and the volatiles were subsequently removed in vacuo from the yellow solution to afford crude product as a light yellow solid. Crystallization of the crude product via vapor diffusion of diethyl ether into a concentrated THF solution yielded analytically pure product as light yellow crystals (37.9 mg, 57.5%). ^{1}H NMR (400 MHz, CD_2Cl_2): δ 7.68 (t, 2H, Ar-*H*), 7.60−7.55 (m, 10H, Ar-*H*), 7.51 (t, 2H, Ar-*H*), 7.46−7.36 (m, 10H, Ar-*H*), 7.09 (t, 2H, Ar-*H*), 7.03 (t, 2H, Ar-*H*), 4.36 (m, 2H, C*H*$_2$), 3.64 (m, 2H, C*H*$_2$), 1.22 (dd, 3H, C*H*$_3$, $^2J_{P-H}$ = 9.2 Hz, $^3J_{Pt-H}$ = 20.8 Hz). ^{31}P NMR (161.8 MHz, CD_2Cl_2): δ 81.5 (dt, 1P, $^1J_{Pt-P}$ = 3411 Hz, $^2J_{P-P}$ = 26.7), −2.5 (dd, 2P, $^1J_{Pt-P}$ = 2220 Hz, $^2J_{P-P}$ = 26.7), −143.9 (sept, 1P, $^1J_{P-F}$ = 710 Hz). ^{13}C NMR (100.5 MHz, CD_2Cl_2): δ 146.0, 137.6, 134.9, 134.4, 132.6, 132.1, 129.3, 128.9, 123.3, 120.3, 46.9, 19.7. Anal. Calcd for $C_{39}H_{35}N_2F_6IP_4Pt$: C, 42.91; H, 3.23; N, 2.57. Found: C, 42.85; H, 3.22; N, 2.50.

[(PP(Me)P)PtI$_2$] (18). Compound **4** (76.5 mg, 0.0746 mmol) was dissolved in 10 mL of dichloromethane. To this yellow solution was added PMe_3 (38.6 μL, 0.373 mmol) and MeI (4.6 μL, 0.075 mmol). The mixture was allowed to stir for 12 h to ensure complete reaction. The yellow precipitate was collected via filtration to afford analytically pure product (65.1 mg, 81.3%). ^{1}H NMR (400 MHz, CD_2Cl_2): δ 7.68 (t, 2H, Ar-*H*), 7.60−7.48 (m, 14H, Ar-*H*), 7.43 (m, 8H, Ar-*H*), 7.07 (t, 2H, Ar-*H*), 7.01 (m, 2H, Ar-*H*), 4.68 (m, 2H, C*H*$_2$), 3.62 (m, 2H, C*H*$_2$), 1.35 (dd, 3H, C*H*$_3$, $^2J_{P-H}$ = 9.2 Hz, $^3J_{Pt-H}$ = 19.2 Hz)). ^{31}P NMR (161.8 MHz, CD_2Cl_2): δ 81.2 (dt, $^1J_{Pt-P}$ = 2259.1 Hz, $^2J_{P-P}$ = 26.7 Hz), −2.8 (dd, $^1J_{Pt-P}$ = 2259.1 Hz, $^2J_{P-P}$ = 26.7 Hz). ^{13}C NMR (100.5 MHz, CD_2Cl_2): δ 146.1, 137.4, 134.8, 134.4, 132.5, 132.1, 129.3, 128.8, 123.1, 120.8, 47.4, 19.4. Anal. Calcd for $C_{39}H_{35}N_2I_2P_3Pt$: C, 43.63; H, 3.29; N, 2.61. Found: C, 43.58; H, 3.26; N, 2.59.

X-ray Crystallography Procedures. All operations were performed on a Bruker-Nonius Kappa Apex2 diffractometer, using graphite-monochromated MoKα radiation. All diffractometer manipulations, including data collection, integration, scaling, and absorption corrections were carried out using the Bruker Apex2 software.[31] Preliminary cell constants were obtained from three sets of 12 frames. Crystallographic parameters are provided in Supporting Information, Tables S1, S2, and S3, and further experimental crystallographic details are described for each compound in the Supporting Information.

Electrochemistry. Cyclic voltammetry measurements were carried out in a glovebox under a dinitrogen atmosphere in a one-compartment cell using a CH Instruments electrochemical analyzer. A glassy carbon electrode and platinum wire were used as the working and auxiliary electrodes, respectively. The reference electrode was Ag/$AgNO_3$ in THF. Solutions (THF) of electrolyte (0.40 M [^{n}Bu$_4$N][PF$_6$]) and analyte (ca. 2 mM) were also prepared in the glovebox.

Computational Details. All calculations were performed using Gaussian09[32] for the Linux operating system. Density functional theory calculations were carried out using the B3LYP hybrid functional, including Becke's parameter exchange functional (B3),[33] and the correlation functional of Lee, Yang, and Parr (LYP).[34] A mixed-basis set was employed, using the LANL2DZ(p,d) double-ζ basis set with effective core potentials for phosphorus, iodine, and platinum[35−37] and Gaussian09's internal LANL2DZ basis set (equivalent to D95 V[38]) for carbon, nitrogen, and hydrogen. Using crystallographically determined geometries as a starting point, the geometries were optimized to a minimum, followed by analytical frequency calculations to confirm that no imaginary frequencies were present. NBO[39] calculations were then performed on the optimized geometries of **4**, **10**, **11*** and their oxidized counterparts. Deletion energies (E^{del}) represent the change in energy upon zeroing the matrix elements corresponding to the lp(Pt)→p(P) donor−acceptor interactions.[40] XYZ coordinates of the optimized geometries of all six complexes are provided in the Supporting Information.

■ ASSOCIATED CONTENT

Supporting Information

Computational details, a scheme describing the formation of **16** and **18**, cyclic voltammetry data, and crystallographic data collection and refinement details and data in .cif format for **1**−**5**, **9**, **11**, **13**, **14**, **16**, and **17**. This material is available free of charge via the Internet at http://pubs.acs.org.

■ AUTHOR INFORMATION

Corresponding Author

*E-mail: thomasc@brandeis.edu.

Notes

The authors declare no competing financial interest.

■ ACKNOWLEDGMENTS

The authors are grateful for startup funds provided by Brandeis University, and C.M.T. is additionally grateful for a 2011 Sloan Research Fellowship.

■ REFERENCES

(1) Arduengo, A. J.; Harlow, R. L.; Kline, M. *J. Am. Chem. Soc.* **1991**, *113*, 361−363.
(2) Crudden, C. M.; Allen, D. P. *Coord. Chem. Rev.* **2004**, *248*, 2247−2273.
(3) Bourissou, D.; Guerret, O.; Gabbai, F. P.; Bertrand, G. *Chem. Rev.* **1999**, *100*, 39−92.
(4) Herrmann, W. A.; Schütz, J.; Frey, G. D.; Herdtweck, E. *Organometallics* **2006**, *25*, 2437−2448.
(5) Marion, N.; Nolan, S. P. *Acc. Chem. Res.* **2008**, *41*, 1440−1449.
(6) Herrmann, W. A. *Angew. Chem., Int. Ed.* **2002**, *41*, 1290−1309.
(7) Bansal, R. K.; Gudat, D. Recent Developments in the Chemistry of N-Heterocyclic Phosphines. In *Phosphorus Heterocycles II*; Springer: Berlin/Heidelberg, Germany, 2010; Vol. *21*, pp 63−102.
(8) Gudat, D. *Coord. Chem. Rev.* **1997**, *163*, 71−106.
(9) Gudat, D. *Acc. Chem. Res.* **2010**, *43*, 1307−1316.
(10) Takano, K.; Tsumura, H.; Nakazawa, H.; Kurakata, M.; Hirano, T. *Organometallics* **2000**, *19*, 3323−3331.
(11) Gudat, D. *Eur. J. Inorg. Chem.* **1998**, *1998*, 1087−1094.
(12) Gudat, D.; Haghverdi, A.; Hupfer, H.; Nieger, M. *Chem.—Eur. J.* **2000**, *6*, 3414−3425.
(13) Hutchins, L. D.; Paine, R. T.; Campana, C. F. *J. Am. Chem. Soc.* **1980**, *102*, 4521−4523.
(14) Hutchins, L. D.; Duesler, E. N.; Paine, R. T. *Organometallics* **1982**, *1*, 1254−1256.
(15) Roncaroli, F.; Videla, M.; Slep, L. D.; Olabe, J. A. *Coord. Chem. Rev.* **2007**, *251*, 1903−1930.
(16) Burck, S.; Daniels, J.; Gans-Eichler, T.; Gudat, D.; Nättinen, K.; Nieger, M. *Z. Anorg. Allg. Chem.* **2005**, *631*, 1403−1412.
(17) Mata, J. A.; Poyatos, M.; Peris, E. *Coord. Chem. Rev.* **2007**, *251*, 841−859.
(18) Peris, E.; Crabtree, R. H. *Coord. Chem. Rev.* **2004**, *248*, 2239−2246.
(19) Day, G. S.; Pan, B.; Kellenberger, D. L.; Foxman, B. M.; Thomas, C. M. *Chem. Commun.* **2011**, *47*, 3634−3636.
(20) Pan, B.; Bezpalko, M. W.; Foxman, B. M.; Thomas, C. M. *Organometallics* **2011**, *30* (21), 5560−5563.
(21) Caputo, C. A.; Brazeau, A. L.; Hynes, Z.; Price, J. T.; Tuononen, H. M.; Jones, N. D. *Organometallics* **2009**, *28*, 5261−5265.
(22) Mazzeo, M.; Lamberti, M.; Massa, A.; Scettri, A.; Pellecchia, C.; Peters, J. C. *Organometallics* **2008**, *27*, 5741−5743.
(23) Caputo, C. A.; Jennings, M. C.; Tuononen, H. M.; Jones, N. D. *Organometallics* **2009**, *28*, 990−1000.
(24) Hardman, N. J.; Abrams, M. B.; Pribisko, M. A.; Gilbert, T. M.; Martin, R. L.; Kubas, G. J.; Baker, R. T. *Angew. Chem., Int. Ed.* **2004**, *43*, 1955−1958.
(25) Mazzeo, M.; Strianese, M.; Kuhl, O.; Peters, J. C. *Dalton Trans.* **2011**, *40*, 9026−9033.
(26) Schneider, S. K.; Roembke, P.; Julius, G. R.; Raubenheimer, H. G.; Herrmann, W. A. *Adv. Synth. Catal.* **2006**, *348*, 1862−1873.
(27) Fürstner, A.; Seidel, G.; Kremzow, D.; Lehmann, C. W. *Organometallics* **2003**, *22*, 907−909.
(28) Dyer, P. W.; Fawcett, J.; Hanton, M. J.; Mingos, D. M. P.; Williamson, A.-M. *Dalton Trans.* **2004**, 2400−2401.
(29) Mihigo, S. O.; Mammo, W.; Bezabih, M.; Andrae-Marobela, K.; Abegaz, B. M. *Bioorg. Med. Chem.* **2010**, *18*, 2464−2473.
(30) Ugo, R.; Cariati, F.; Monica, G. L.; Mrowca, J. J., Tris- and Tetrakis(Triphenyl-Phosphine)Platinum (0). In *Inorganic Syntheses*; John Wiley & Sons, Inc.: New York, 2007; pp 105−108.
(31) *Apex 2*, Version 2 User Manual, M86-E01078; Bruker Analytical X-ray Systems: Madison, WI, 2006.
(32) Frisch, M. J.et al. *Gaussian 09*, Revision A.1; Gaussian, Inc.: Wallingford, CT, 2009.
(33) Becke, A. D. *J. Chem. Phys.* **1993**, *98*, 5648−5652.
(34) Lee, C.; Yang, W.; Parr, R. G. *Phys. Rev. B* **1988**, *37*, 785−789.
(35) Hay, P. J.; Wadt, W. R. *J. Chem. Phys.* **1985**, *82*, 299−310.
(36) Hay, P. J.; Wadt, W. R. *J. Chem. Phys.* **1985**, *82*, 270−283.
(37) Wadt, W. R.; Hay, P. J. *J. Chem. Phys.* **1985**, *82*, 284−298.
(38) Dunning, T. H.; Hay, P. J. In *Modern Theoretical Chemistry*; Schaefer, H. F., Ed.; Plenum: New York, 1976; Vol. 3, pp 1−28.
(39) Glendening, E. D.; Reed, A. E.; Carpenter, J. E.; Weinhold, F. *NBO*, Version 3.1.
(40) Reed, A. E.; Curtiss, L. A.; Weinhold, F. *Chem. Rev.* **1988**, *88*, 899−926.